

Decomposition and heat distributions of a designed propellant formulation

ZHANG QIUYAN, SONG QIANG

Electric Power Research Institute of Guizhou Power Grid Co., Ltd

In this paper, the effects of heat loss on the micro motor performance were investigated, and the propellant formulation was screened to meet the requirements of micro motor. For a designed binder, with the increase of nitrocellulose content, the thermal decomposition performance of LS/NC was the best, the thermal decomposition performance of AP/NC was the worst, and 5:5 LS/NC was suitable as a micro solid rocket propellant formulation. Further calculations demonstrated that the highest temperature appeared at the boundary of the combustion chamber, where the thermal stress and deformation were the maximum. The heat loss had great effects on micro-thruster performance, and the thrust of micro-thruster decreased by 21.7%, and specific impulse decreased by 11.8%. The maximum equivalent thermal stress and thermal deformation of single motor wall were 134.2Mp and 305.9nm respectively. The maximum thermal deformation was small and had little effect on the thermal stability, whereas the thermal stress was the main reason for the stability destruction.

(Received May 25, 2015; accepted June 09, 2016)

Keywords: Decomposition, Propellant

1. Introduction

MEMS-based solid propellant micro-thruster has broad applications for small satellites operating at high altitude and orbit control technology because of its small size, high precision micro impulse and good integration [1-2]. The combustion in micro motor is very different from the main motor, because the surface area / volume increases rapidly, rheological effects are obvious, heat loss is large, so that the temperature of the internal flowing fluid more obvious increases, thereby affecting their flow and heat transfer.

In 2007, Louisos and Hitt [3] of the University of Vermont, USA studied viscous flow and the heat transfer loss of 2D and 3D supersonic linear micro nozzle by CFD software, it was found that there existed an intrinsic exchange between the viscous losses and losses which generated due to non-axial exports flow. In the three-dimensional simulation, because of the presence of longitudinal flat wall, the adhesive effect was more significant; the viscosity effect can be reduced because of the heat loss generated by flow and a corresponding reduction of subsonic boundary dimensions, thus improving the performance of the micro nozzle. In 2009, the reason why the heat loss can improve the micro-nozzle thrust was studied by Louisos and Hitt [4], they presented three reasons: the gas flow heat exchange reduced subsonic viscous layer area; Rayleigh flow acceleration; The heat transfer of fluid to the substrate increased the gas density. In 2010, José Antonio Morínigo and José Hermida-Quesada [5] solved NS equations by using second-order slip boundary model and gas - solid thermal coupling model to study the effects of the interaction of the gas and the wall on the micro nozzle performance, they proved that solid wall had a huge impact on the flow of

gas, and thus the performance of the micro nozzle. In 2011, in order to reduce the heat loss caused by subsonic boundary layer, the nozzles which expand half-angle were 15 ° and 30 ° was designed by numerical simulations by Cheah and Chin, so that the micro-nozzle performance increased by 5% than the traditional linear nozzle. In the domestic institutions which engaged in micro-thruster flow field were mainly Tsinghua University, China University of Technology, and Nanjing University of Technology. In 2003, simulation of the combustion in micro turbine annular combustion chamber was carried by using CFD software by Li [7], Jiangsu University to analyze the factors effecting the combustion, he proposed the efficient ways and means to reduce heat loss and improve the micro-combustor. The gas flow process and heat loss of the two solid micro-thruster structure were simulated by Zhou, Tsinghua University, he proposed the method which improved the impulse performance of micro-thruster by using glass or ceramic materials with good insulation properties. In 2006, a heat transfer model was established based on the actual working conditions of micro rocket motor by Zhou [9], Nanjing University of Science & Technology, which served as a basis for calculating the transient temperature field of motor work. Comparison of temperature distribution was made on systems with copper, iron and aluminum shell material, the results showed that the copper shell can be kept at relatively low temperatures, the temperature of the rear part of grain burning surface near the insulating layer would increase to a different level, which had an impact on the burning rate and can easily lead to unstable combustion. The influences of units number, gas temperature, reaction time and the array structure on micro-thruster combustion chamber thermal stress and thermal deformation were simulated by the ANSYS coupled transient thermal structure calculation

methods by Liu [10], Nanjing University of Science & Technology. The results showed that: the maximum thermal stress and thermal deformation of the hole was mainly concentrated in the combustion chamber boundary where is the weakest part of the structure; compared with a single unit, the equivalent thermal stress was large on the effect of the array, the maximum deformation was smaller; The maximum equivalent thermal stress and maximum deformation increased with the increases of gas temperature, the time and chamber diameter, decreased with the increases of array element spacing. In 2003, the influence of micro scale effects and flow loss on the thrust-time curve during the transient work process of thruster which combined dynamic mesh and fluid-solid coupled heat transfer model was studied by Li [11], Beijing Polytechnic University. The results showed that for the study micro-thruster, micro scale effects had a significant effect on flow field, but had little effect on the thrust. The main factors affecting the thrust trend curve was heat loss trend in the hypothesis that the propellant measured burning rate was under stable combustion. The overall heat loss of micro-thruster was small by using Mecor Corning Ceramic materials and decreased with time, while the overall heat loss of micro-thruster was large for Si material and increased with time.

In this paper, a suitable propellant formulation was selected through energy characteristics and thermal decomposition characteristic; Thermal analysis calculation of the micro-thruster array was carried out, temperature distribution, thermal stress and thermal deformation of the thruster array with the combustion chamber materials of silicon and steel was comparatively studied; A monopropellant engine physics and mathematics micro model was established, a three-dimensional numerical simulation was carried out, the impact of heat loss on motor performance was studied.

2. Selection of propellant formulation for the micro motor

A. Energy characteristics of propellants

Due to the simple structure, less charge, and electric ignition of micro motor, it is impossible to use the traditional point pyrotechnic device, thus the charge was required to be more sensitive to electro thermal, and to be easily ignited directly under electric conditions, solid propellant used for micro-thruster is quite different from common propellant, a high energy, high heat-sensitive characteristics, shorter ignition delay time, the excellent filling performance were required. Ammonium Perchlorate (AP)/Nitrocellulose (NC), Lead Dinitramide (LD)/Nitrocellulose, Lead Styphnate (LS)/Nitrocellulose compositions were selected as propellants, energy characteristics and thermal decomposition characteristics analysis of the different propellant formulations will be carried out to select the best formulation.

Thermodynamic calculations of the combustion chamber and nozzle were performed using the Minimum Gibbs free energy method to get some parameters that represent energy characteristics of the propellants. Thermodynamic calculation conditions as follows; Initial temperature was set to room temperature at 300 K, the initial pressure of the combustion chamber was set to the atmospheric pressure 1MP, the combustion chamber area and nozzle throat area $A_c/A_t = 1^2/0.246^2 = 16.52$, nozzle expansion ratio $A_e/A_t = 0.6^2/0.246^2 = 5.95$. Table 1 given below gives the energy characteristic parameters of the four types of propellants in different proportion.

Table 1. The energy characteristic parameters of propellants.

Propellant	Code	Ratio	Energy Characteristics				
			T_f/K	n_g /mol·kg ⁻¹	γ	$I_{sp}/N \cdot s \cdot kg^{-1}$	$C^*/m \cdot s^{-1}$
LS/NC	A1	8:2	2738.5	24.2	1.1	2087.2	1190.1
	A2	7:3	2715.7	26.1	1.1	2150.3	1226.3
	A3	6:4	2695.3	28.0	1.1	2211.7	1261.4
	A4	5:5	2676.8	29.9	1.1	2271.6	1295.4
LD/NC	B1	8:2	1529.7	22.0	1.1	1522.7	864.6
	B2	7:3	1603.5	24.7	1.1	1667.3	941.8
	B3	6:4	1849.9	27.3	1.1	1811.6	1016.8
	B4	5:5	2051.2	29.7	1.1	1954.2	1106.9
AP/NC	C1	8:2	2347.3	34.7	1.2	2150.9	1246.3
	C2	7:3	2594.0	34.2	1.2	2217.3	1316.3
	C3	6:4	2725.1	33.6	1.2	2310.2	1412.1
	C4	5:5	2815.7	33.0	1.2	2375.9	1488.9

From Table 1 we can conclude that

(1) Comparing A1, B1, C1, they all contain the same number and variety of binder NC, the C^* (Characteristic

velocity) of C1 is 1246.3 m/s which is 56.2m/s higher than the value for A1 and 381.7m/s higher than the value for B1, the specific impulse I_{sp} of C1 is 63.7N·s/kg higher than

A1 and 598.2 N·s/kg higher than B1. It can be seen that with the same binder and content, AP propellant has higher energy, which indicates that the improvement of propellants energy by AP is more pronounced. Fig. 1 shows that the impulse changes of different formulation propellants, it can be drawn from this figure, with the same binder conditions, energy of the propellant with oxidizer AP is higher than that with oxidizers LS or LD, and energy of the propellant with oxidizer LD is minimum. The same conclusion can be draw by comparing respectively A2, B2 and C2, A3, B3 and C3, A4, B4 and C4;

(2) Comparing A1, A2, A3 and A4, represents an increase of the content of NC in the propellant from 20% to 50%, the C* and specific impulse are both increased. This shows that increasing the content of NC can improve propellant energy, when the content of NC is 50%, the propellant energy is the highest; The same conclusion can be drawn by comparing B1, B2, B3 and B4, and also C1, C2, C3 and C4 respectively. From Fig. 1, it can more clearly see the trends of specific impulse.

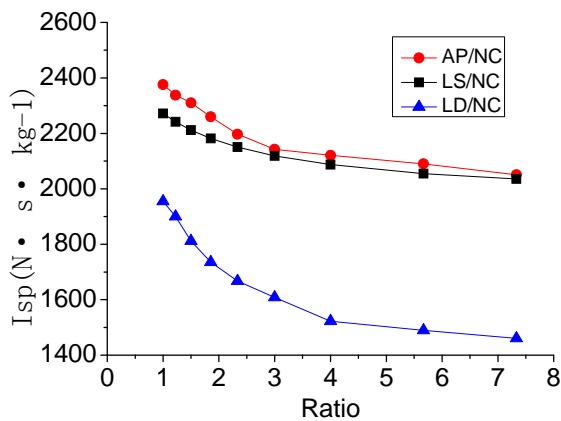


Fig. 1. Specific impulse changes of different formulations propellants.

The above analysis shows that in the same binder, energy of AP propellant system is higher than corresponding LS propellant system; and for LS propellant system the energy is higher than corresponding LD propellant system; energy of the propellant can be improved with increase of NC.

Since the size of solid micro-thruster is very small, and it uses heating resistance wire or semiconductor bridge ignition, its charge requires the propellant to have a high thermal characteristic, short ignition delay time, excellent loading performance and other conditions. Secondly, because the micro-thruster drug chamber is small, typically is sub-millimeter, and with further research and the increase the degree of drug chamber integration, the diameter of the drug is bound to get smaller, the dimensionless requires ignition agents critical conditions as small as possible to avoid the hard ignition in the small-diameter appears. So the thermal decomposition characteristics of propellant will be further studied.

B. Thermal decomposition characteristics of propellants

The DSC experiments were conducted to study the thermal decomposition characteristics of micro-propellant. To comparing the thermal decomposition characteristics of different propellant formulations, the different ratio of LS/NC propellant, LD/NC propellant and AP/NC propellant were designed as shown in Table 2.

Table 2. Tested propellant formulations

Propellant Formulation	Ratio			
LS/NC	5:5	6:4	7:3	—
LD/NC	5:5	6:4	7:3	—
AP/NC	5:5	6:4	7:3	8:2

Fig. 2-4 are DSC thermal decomposition curves of different ratios LS/NC, LD/NC, AP/NC. The first decomposition peak is the decomposition of NC, the second decomposition peak is the decomposition of oxidizer. The following figure shows that the exothermic peak of LS is relatively sharp, indicating the decomposition of LS is accompanied with a lot of heat in a very short period of time, the decomposition peak temperature is 257.5°C, the decomposition of LD is slower than LS, the decomposition peak temperature is 266.4°C, the decomposition peak temperature of AP is 380.2°C, thermal decomposition peak temperature of LS/NC in three micro-propellant is minimum, indicating LS/NC had the best performance of thermal decomposition, whereas AP/NC was the worst.

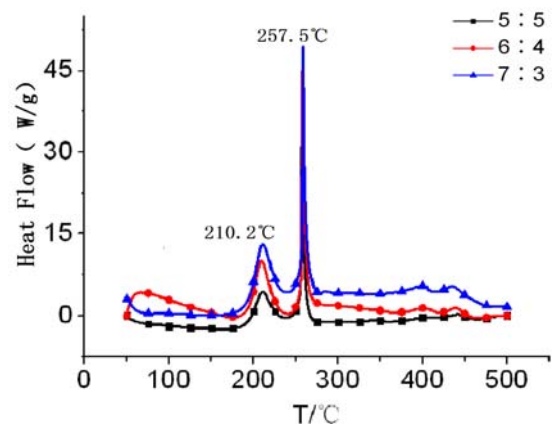


Fig. 2. DSC curve of LS/NC (7:3, 6:4, 5:5).

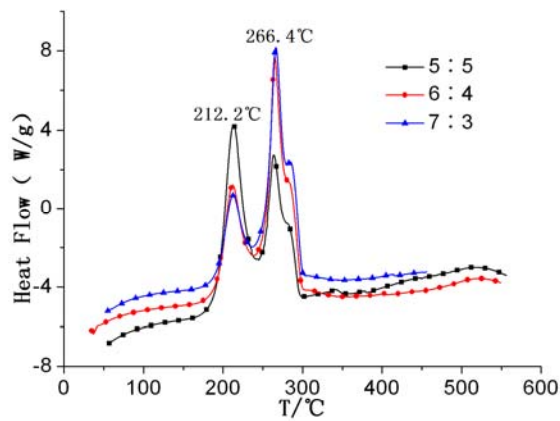


Fig. 3. DSC curve of LD/NC (7:3, 6:4, 5:5).

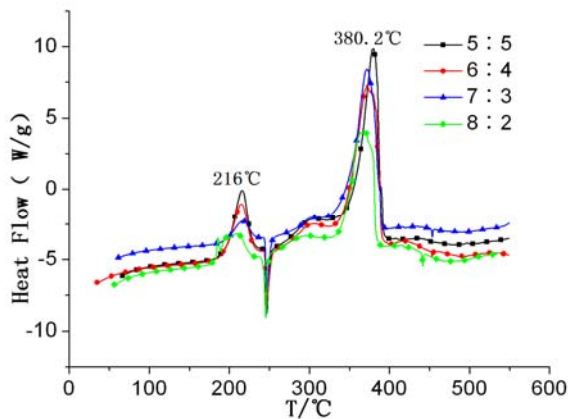


Fig. 4. DSC curve of AP/NC (8:2, 7:3, 6:4, 5:5)

According to the micro solid motor requirements of propellant and complete energy characteristics and the thermal decomposition characteristics of the results, the high energy and high heat-sensitive, 5:5 LS/NC was most suitable as a micro solid rocket propellant formulations. So the influence of heat loss on the combustion shell and motor performance will be studied by using this propellant formulation.

3. Influences of heat loss on combustion chamber shell

A. Research scheme

The transient temperature distribution of thrusters array whose drug chamber materials were silicon and steel respectively were calculated through thermal stress coupled transient indirect analysis method by the finite element analysis software, Ansys, and then thermal stress distribution and deformation were calculated by the thermal structure coupled. The propellant was 5:5 of LS/NC, thermodynamic parameters of the gas were calculated by minimal Gibbs free energy method, the gas

temperature was 2000K. The density of silicon was 2300kg/m^3 , the heat capacity was $700\text{J/kg}\cdot\text{K}$, the thermal conductivity was $160\text{W/m}\cdot\text{K}$, the linear expansion coefficient was $4.15\cdot 10^{-6}\text{K}^{-1}$, the elastic modulus was 131GPa , Poisson's ratio was 0.27. The density of steel was 7850kg/m^3 , the heat capacity was $480\text{J/kg}\cdot\text{K}$, the thermal conductivity was $48\text{W/m}\cdot\text{K}$, the linear expansion coefficient was $1.2\cdot 10^{-5}\text{K}^{-1}$, the elastic modulus was 210GPa and the Poisson's ratio was 0.28.

In this paper the 4×4 array thruster was shown in Fig. 5. After the propellant grain was filled in the combustion chamber, the combustion chamber and nozzle are bonded together to form a complete miniature solid engine structure. Since the heat effect of micro-thruster drug chamber is the largest and most unstable during work process, so the drug chamber layer will be studied, the drug chamber diameter is 1mm, cell spacing is 0.6mm.

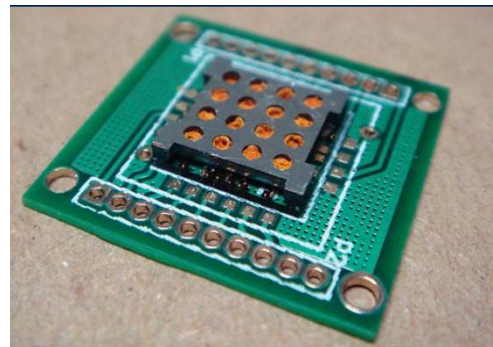


Fig. 5. Photo of micro thruster

B. Meshing and boundary conditions

Since the drug chamber layer was structurally symmetric, in order to facilitate the calculation, only 1/4 of four drugs chambers were computational analyzed, as shown in Fig. 6, the calculation region was divided by using a structured grid. Model boundary conditions was the symmetric boundary, plus a fixed constraint, 1,2,3,4 was the boundary of drug chamber hole, gas and drug chamber wall had thermal effect, the heating load is in 1,2,3,4, boundary conditions were set as the third boundary condition. Initial drug chamber temperature was 300K.

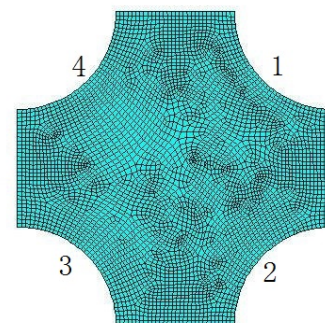


Fig. 6. Grid graph of micro-thruster array drug chamber

C. The analysis of simulation results

The initial temperature of the wall was 300K, the calculation time was 5ms, Fig. 7 and Fig. 8 are the temperature distribution of drug chamber layer at 5ms, the figure shows that the highest temperature in both two materials are in the drug chamber hole boundary, the maximum temperature of the silicon material drug chamber is 333.613K. The maximum temperature of the silicon material drug chamber is 327.235K. It can be seen that the temperature gradient of steel shell is larger by comparing Fig. 7 and 8, which was due to the worse thermal conductivity of steel than silicon, the time required to establish thermal equilibrium was longer. The temperature curves of edges of the hole were taken, Fig. 9 is the temperature curve versus time of drug chamber hole boundary, it can be seen that at the edges of the two materials hole temperatures are increasing with time, the heating of silicon material drug chamber hole is faster than that of the steel, which was due to the greater thermal conductivity of silicon, more heat conduction per unit time.

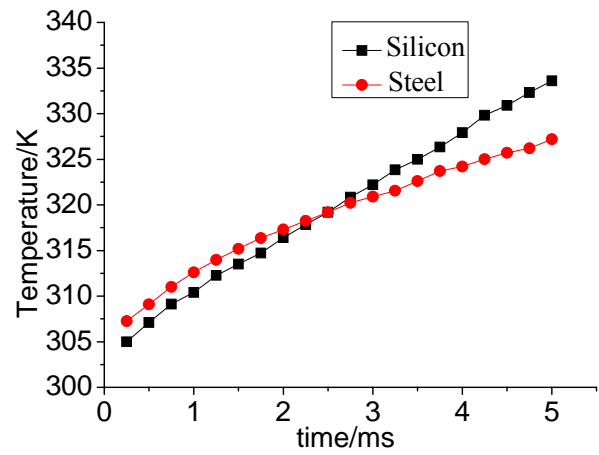


Fig. 9. Temperature-time curve of combustion chamber hole boundary

The following figures are the equivalent thermal stress and deformation distribution under the conditions of two shell materials at 5ms, the figure shows that the maximum equivalent thermal stress and maximum thermal deformation have occurred at the boundary of combustion chamber hole.

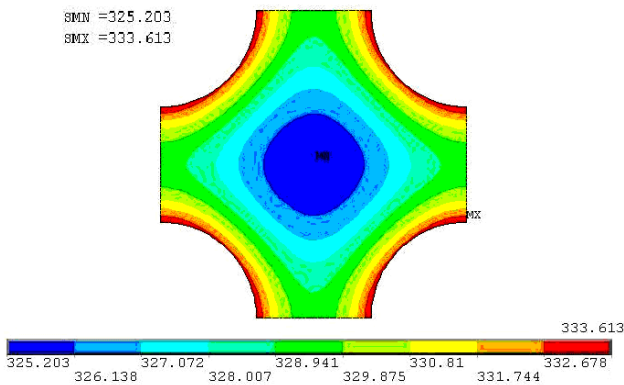


Fig. 7. Temperature distribution of silicon material combustion chamber at 5ms

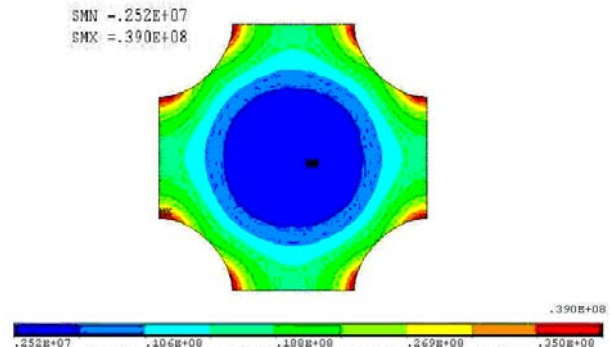


Fig. 10. Thermal stress of silicon material combustion chamber at 5ms

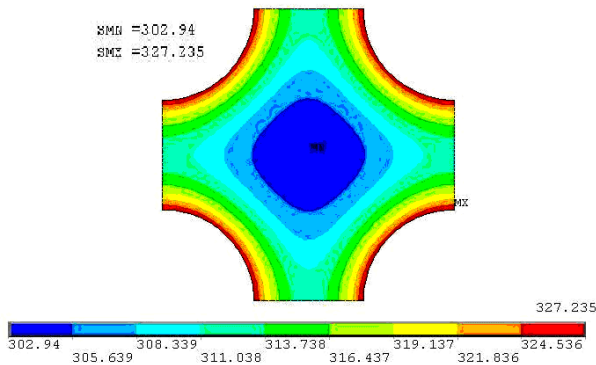


Fig. 8. Temperature distribution of steel material combustion chamber at 5ms

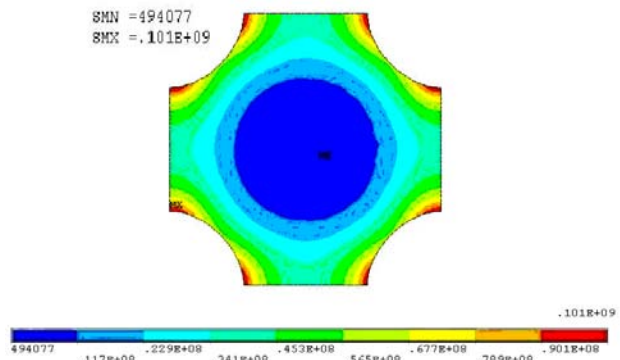


Fig. 11. Thermal stress of steel material combustion chamber at 5ms

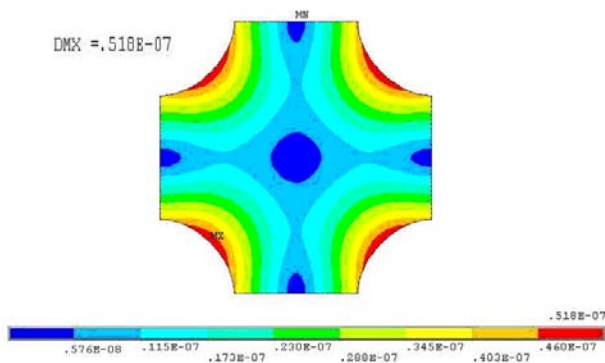


Fig. 12. Deformation of silicon material combustion chamber at 5ms

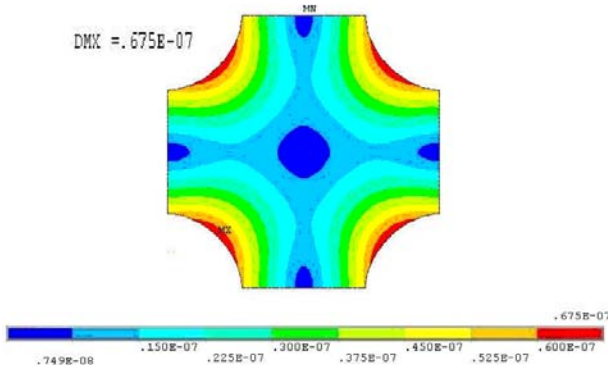
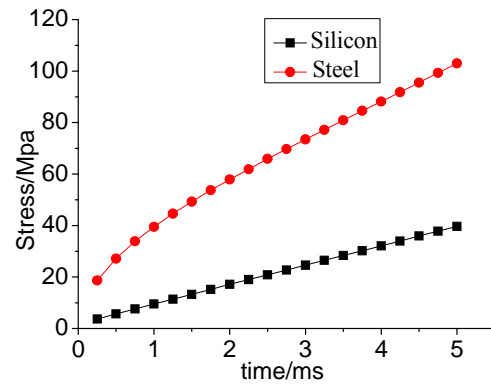
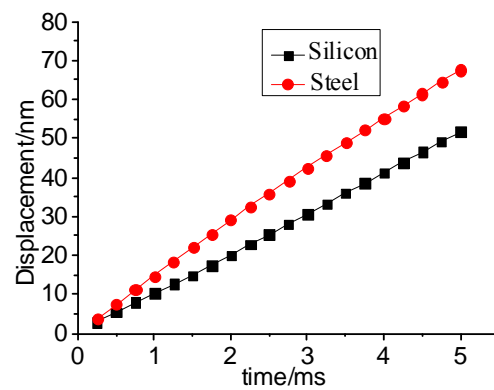


Fig. 13. Deformation of steel material combustion chamber at 5ms

Respectively, Fig. 14 (a) (b) are the equivalent thermal stress and deformation curves over time under the conditions of two shell materials, the figure shows that the maximum equivalent thermal stress and maximum deformation of two material shells increased over time, with the increase of the action time, the heat entered the combustion chamber wall in a long time and heat conduction distance was farther, so that the thermal stress and deformation became larger. The maximum equivalent thermal stress and thermal deformation of the micro-thruster with silicon material shell are 39Mpa and 51.8nm, the maximum equivalent thermal stress and thermal deformation of the micro-thruster with steel material shell are 101Mpa and 67.5nm, which is significantly greater than silicon. This was because the thermal conductivity of silicon was better, it was easier to establish thermal equilibrium, the temperature gradient of the shell was small, and the elastic modulus and the linear expansion coefficient were less than steel, resulted in a smaller effect of stress and deformation.



a) thermal stress



b) deformation

Fig. 14. The equivalent thermal stress and deformation curves over time under the conditions of two shell materials

4. Influences of heat loss on micro thruster performance

With the reduction of micro motor size, the ratio of the area-volume is increased, the Reynolds number of the micro nozzle was particularly low (generally less than 1000), the viscous dissipation was particularly serious, and the heat conduction of high temperature gas to wall was serious; The reduction of motor size increased the internal temperature gradient of wall, and further increase the heat loss, and the heat loss of wall not only lead to reduction of motor thrust, but also affected the combustion efficiency and thermal efficiency of the entire micro power system, in this paper the influence of wall heat loss on motor performance was studied by using numerical simulations.

A. Calculation model and boundary conditions

The calculation model structure size is shown in Fig. 15, when the influence of the heat loss on motor performance was calculated. Combustion chamber is a round hole type, nozzle cross-sections are square, contraction segment and expansion segment are rectangular pyramid.

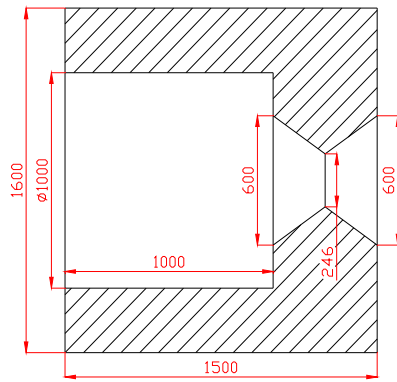


Fig. 15. Calculation model structure size

For the N-S equation, its solution is unique only under certain initial and boundary conditions, the boundary conditions largely affect the stability of the numerical calculations, if handled properly, resulting in numerical results does not converge, or even diverge. On the other hand, processing of the boundary conditions has a very significant impact on the accuracy of the flow field. In order to improve the accuracy of the flow field, it is necessary to improve the processing accuracy of border format, so that the format accuracy of the boundary and inside matches.

During the flow field numerical simulation, the following types of boundary conditions were used:

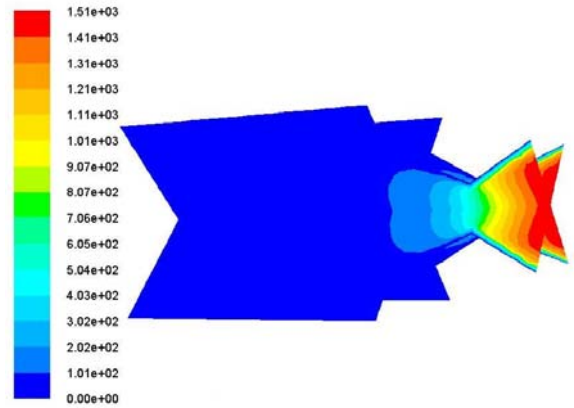
(1) Inlet boundary conditions: The mass flow rate conditions used at inlet boundary are, the mass flow rate of the balance paragraph is 0.15g/s. Propellant is 5:5 of LS/NC. Therefore, the gas is assumed as ideal gas, calculation from the minimization Gibbs free energy method has been carried: the thermal conductivity of the gas is 0.71035 W/m·K, the specific heat is 2447 J/kg·K and viscosity coefficient is $1.0086 \times 10^{-4} \text{Pa}\cdot\text{s}$;

(2) Outlet boundary conditions: Pressure outlet conditions is used at nozzle exit, the outlet pressure is 1000Pa;

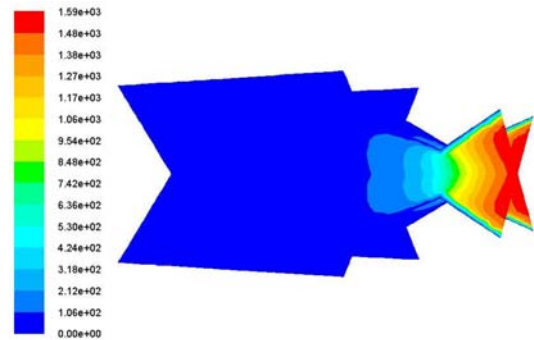
(3) Wall boundary conditions: in consideration of the heat insulating case, slip-free wall is used. In consideration of heat loss, the wall of the gas-solid contact with, the thermal coupled interface is used, the velocity is no-slip condition.

B. Analysis of simulation results

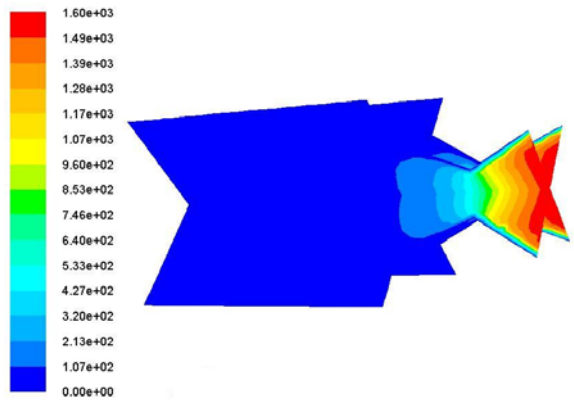
In order to investigate the impact of heat loss on thruster performance, the appropriate turbulence model was selected, in this paper the side length of thruster throat was 246 μm during combustion simulation, a comparative analysis of combustion and flow in the micro-thruster was studied under adiabatic conditions and heat dissipation conditions, the working time was 5ms, Fig. 16 is the velocity figure of micro-thruster at each time under heat dissipation conditions.



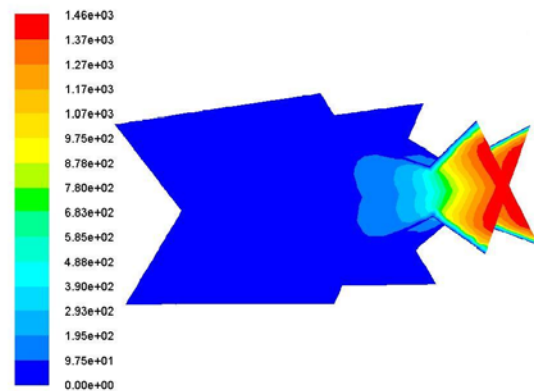
a) Velocity figure at 1ms



b) Velocity figure at 2ms



c) Velocity figure at 3.5ms



d) Velocity figure at 4.5ms

Fig. 16. (a) (b) are the velocity figure at 3ms under adiabatic and heat dissipation conditions.

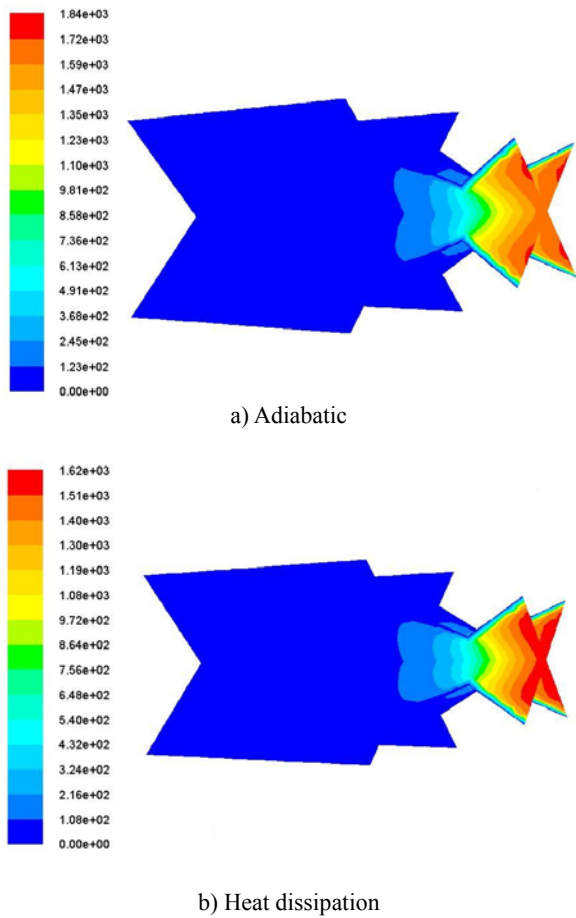


Fig. 17. Velocity figure of micro-thruster at 3ms under two conditions.

Fig. 17 is a comparison of the Mach number distribution along X-axis at the nozzle center line under the two conditions at 3ms. Fig. 18 is a comparison of the Velocity distribution along the Y-axis at the nozzle outlet under the two conditions at 3ms.

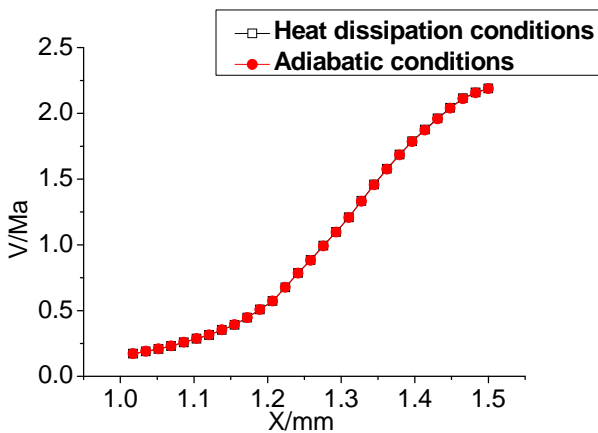


Fig. 18. Velocity of micro nozzle axis at 3ms

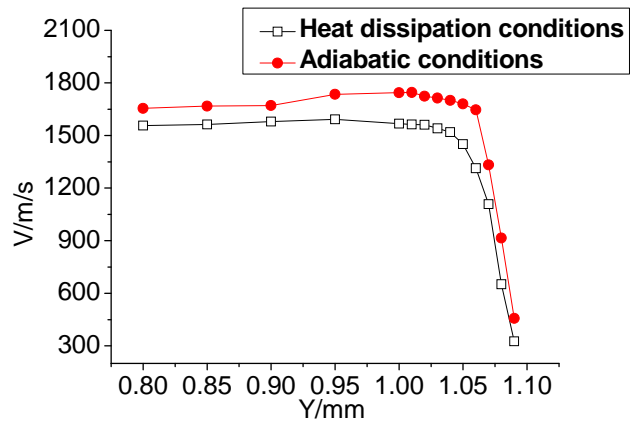
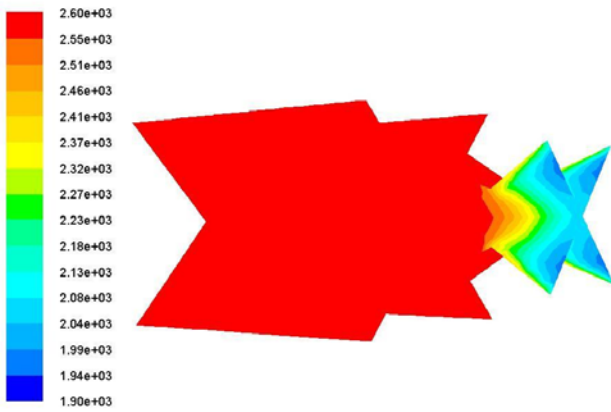


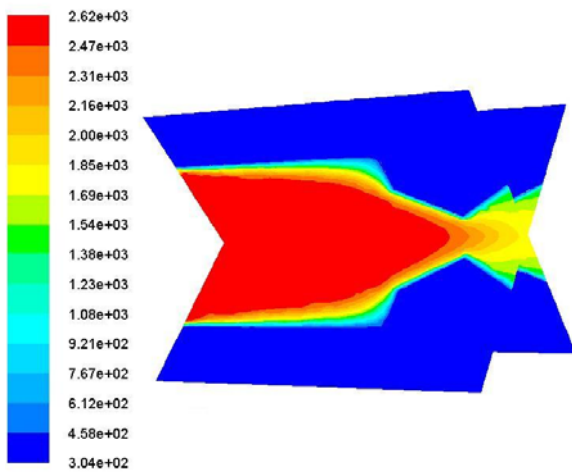
Fig. 19. Velocity along the Y-axis at the nozzle outlet at 3ms

The velocity change of micro-thruster during the work process is shown in Fig. 16. It can be known that velocity distribution at 3ms under the two conditions is similar, the maximum velocity under heat dissipation conditions is 1620m/s, the maximum velocity under adiabatic conditions is 1840m/s. Fig. 18 shows that the Mach number along the centerline of the nozzle has little difference, exit mach number is 2.3Ma, it can be seen from Fig. 19, the velocity close to the wall at the nozzle exit under adiabatic conditions is lower than heat dissipation conditions, it was because of the heat transfer of gas to the solid wall, which resulted in the motor heat loss, especially the heat loss near the wall was higher, the temperature contours in Fig. 20 can also be seen that gas heat transfer to the wall led to the wall temperature higher.

Fig. 22 shows that the micro-thrust under adiabatic conditions at 3ms is 202mN, after adding wall to the chamber shell, the thrust is 166mN, compared with the adiabatic conditions, the thrust peak was lowered by 21.7%, the specific impulse under adiabatic conditions is 1683.7 N·s/kg, the specific impulse under heat dissipation conditions is 1485.2 N·s/kg, a decrease was 11.8%, which was due to the heat loss caused by thermal conductivity of the high temperature gas to the wall, resulted in the decrease of thrust and specific impulse. It also describes that the heat loss due to heat transfer had to be dealt with, because it affected the performance of micro-thruster. If the conditions are favorable, glass ceramics and other materials can be used to reduce the heat loss.



a) Adiabatic



b) Heat dissipation

Fig. 20. Temperature figure of micro-thruster at 3ms under two conditions

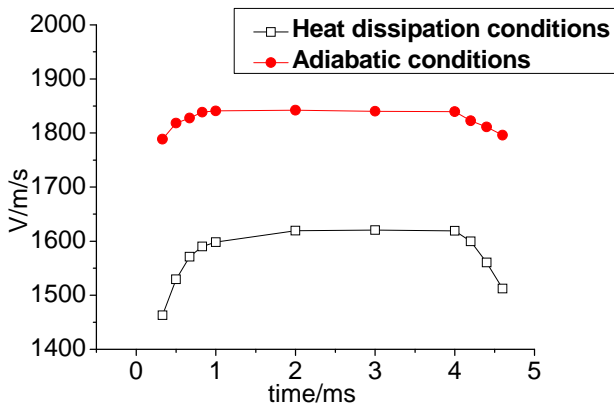


Fig. 21. The maximum velocity-time curve at micro nozzle exit

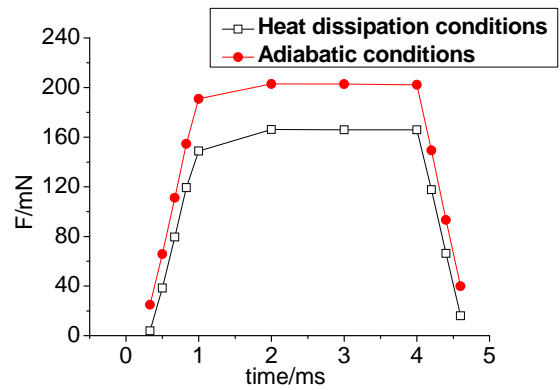


Fig. 22. The thrust-time curve at micro nozzle exit

Fig. 23 is the temperature distribution under heat dissipation conditions, the maximum wall temperature is 472.83K, which was due to heat transfer of gas to solid wall, it resulted in the higher wall temperature, the temperature gradient can be clearly seen along the wall, and throat temperature was higher at the gas inlet.

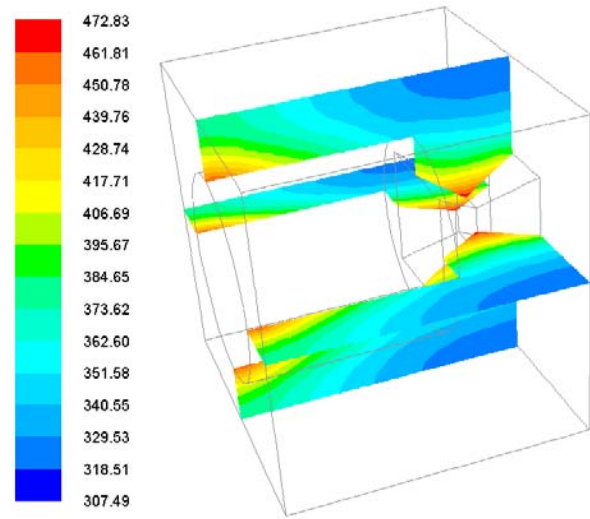


Fig. 23. Temperature figure of micro-thruster under heat dissipation conditions

Figs. 24 and 25 are the equivalent thermal stress and thermal deformation distribution of the micro-thruster structure. The maximum equivalent thermal stress and deformation are 134.2Mpa and 305.9nm respectively. The higher the temperature at the wall, the greater the equivalent thermal stress, it was because the more heat conducted to the drug chamber, the higher the wall temperature was, resulted in a large temperature difference between the wall in the same action time, and within a certain time, the relationship of thermal stress and temperature difference (T-T₀) was:

$$\sigma = -\alpha E (T - T_0) \tag{1}$$

It can be seen from the formula that thermal stress and the temperature difference of the object was directly proportional when the thermodynamic properties of material was the same, the thermal stress generated by the temperature was proportional to the wall temperature, the increase of gas temperature not only had a bigger influence on the combustion chamber, but also led to the increase of deformation. The maximum thermal deformation of micro-thruster is small, had little effect on the thermal stability, the maximum equivalent thermal stress was high, which was the main reason for the destruction of micro-thruster stability.

The maximum thermal stress occurred at the inlet of the gas, this was because the external constraints interaction internal constraints so that deformation generated blocked when temperature of the object was change, the thermal stress generated. With the same temperature changes, the greater the constraints acted on the object, the greater the thermal stress was. Combustion chamber inlet surface covered with ignition layer was fixed constraints, and the wall temperature was high, resulted in the maximum thermal stress.

The maximum thermal deformation occurred at the nozzle outlet, because the constraints of combustion chamber inlet surface was large, which limited the deformation, and the nozzle outlet surface was freely deformable, so deformation of the nozzle outlet was larger.

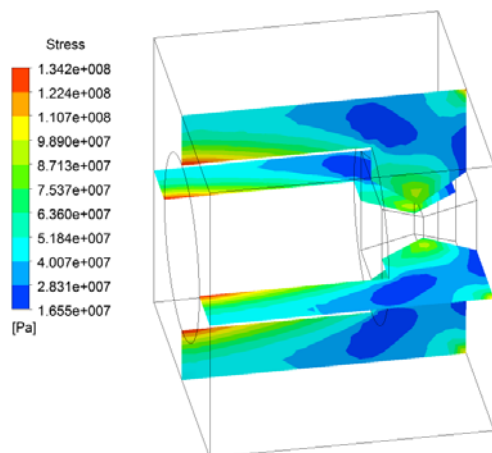


Fig. 24. Equivalent thermal stress distribution of micro-thruster

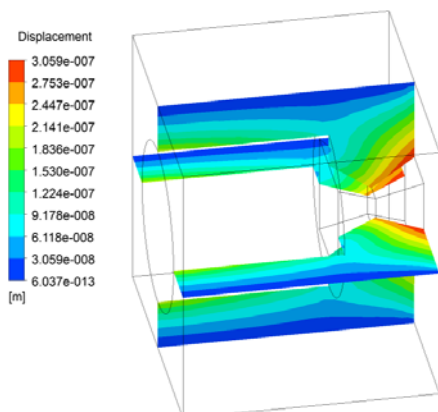


Fig. 25. Thermal deformation distribution of micro-thruster

Fig. 26 are the maximum equivalent thermal stress and maximum deformation curves of micro-thruster inlet, nozzle outlet, throat over time, and the figure shows that the maximum equivalent stress and maximum thermal deformation increases with time and finally stabilized. With the increase of gas reaction time at the initial stage, the heat passing long wall drugs, the heat passed to the wall in a long time, the wall temperature became higher, and heat conduction distance was farther, when the heat transferred in a period of time, the wall gradually established thermal equilibrium, the wall temperature gradient reduced, the equivalent thermal stress and deformation was stabilized.

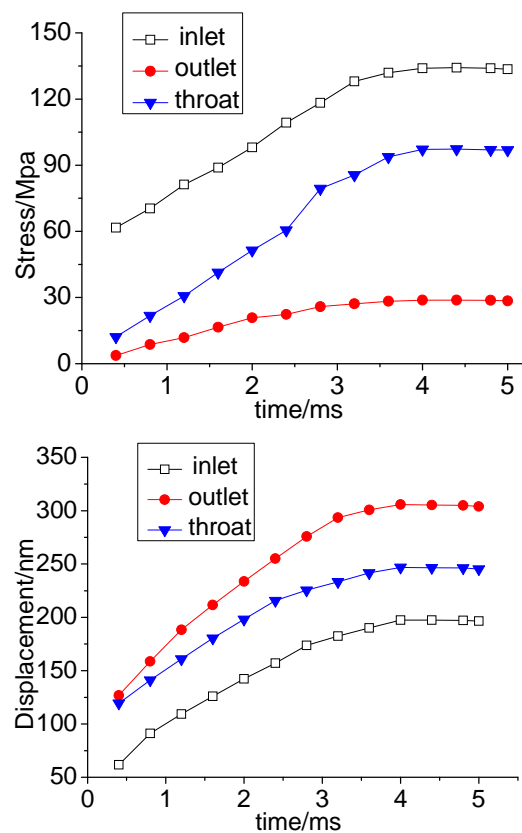


Fig. 26. The maximum equivalent thermal stress and maximum deformation curves of micro-thruster inlet, nozzle outlet, throat over time

5. Conclusions

In this paper propellant formulation was screened to meet the requirements of micro motor to study the effects of heat loss on the combustion chamber shell, micro motor performance. The results showed that:

(1) With the same binder, energy of the Ammonium Perchlorate propellant system was greater than the Stephen Lead propellant system, Stephen Lead propellant system was higher than Lead Dinitramide system; With the

increase of nitrocellulose content, propellants energy can improve; The thermal decomposition performance of LS/NC was the best, The thermal decomposition performance of AP/NC was the worst; 5:5 LS/NC was suitable as a micro solid rocket propellant formulation.

(2) Simulation results of micro motor array showed that the highest temperature appeared at the boundary of the combustion chamber, where the thermal stress and deformation were the maximum; The maximum equivalent thermal stress and thermal deformation of the micro-thruster array with silicon material shell are 39Mpa and 51.8nm, the maximum equivalent thermal stress and thermal deformation of the micro-thruster array with steel material shell are 101Mpa and 67.5nm.

(3) A single thruster with a side length of the throat $246\ \mu\text{m}$ was calculated by unsteady three-dimensional numerical simulation, respectively a comparative analysis was made in insulation and heat loss conditions. The thrust of micro-thruster decreased by 21.7%, specific impulse decreased by 11.8%, which caused by heat loss, the heat loss had great effects on micro-thruster performance.

(4) The maximum equivalent thermal stress and thermal deformation of single motor wall were 134.2Mp and 305.9nm respectively, the maximum thermal deformation was small, which had little effect on the thermal stability, the thermal stress was large which was the main reason for the destruction of micro-thruster stability.

References

- [1] Darren L. Hittl, CharlesMZakrzwski, Michael A. Thomas, *Smart Materials and Structures*, **10**(2), 1163 (2001).
- [2] Norman Chigier, Tevfik Gemci, *American Institute of Aeronautics And Astronautics*, **670**(2), 1 (2003).
- [3] W. F. Louisos D. L. Hitt, In: 37th AIAA Fluid Dynamics Conference, Miami, FL, 2007.
- [4] W. F. Louisos, D. L. Hitt, In: 39th AIAA Fluid Dynamics Conference, San Antonio, Texas, 2009.
- [5] José Antonio Morí ñigo, José Hermida-Quesada, *Sensors and Actuators A: Physical*, **162**(1), 61 (2010).
- [6] K. H. Cheah, J. K. Chin, *Acta Astronautica*, **69**(1-2), 59 (2011).
- [7] Li Taode, Pan Jianfeng, *Journal of Combustion Science and Technology*, **9**(2), 183 (2003).
- [8] Zhou Haiqing, Zhang Gaofeng, You Zheng, *Journal of Propulsion Technology*, **28**(3), 230 (2007).
- [9] Zhou Chao, Zheng Ya, Zhou Changsheng, *Journal of Projectiles; Rockets; Missiles and Guidance*, **26**(2), 1166 (2006).
- [10] Liu Jian, Ye Yinghua, Shen Ruiqi, *Chinese Journal of Energetic Materials*, **17**(3), 357 (2009).
- [11] Li Teng, Fang Shuzhou, Liu Xuhui, *Journal of Solid Rocket Technology*, **36**(5), 613 (2013).
- [12] Zhu Chuazheng, Xu Haihan, *Physical Chemistry. Bei Jing: Science Press*, 163 (2000).
- [13] V. N. Dan, G. Susana, L. Eduardo, *Computers and Chemical Engineering*, **26**(3), 1703 (2002).
- [14] Xia Jiancai, Beijing: Beijing Institute of Technology Press, 2009.

*Corresponding author: liujifu2@126.com